

Loads and motions for a spar-supported floating offshore wind turbine

Abhinav Sultania and Lance Manuel*

Department of Civil, Architectural and Environmental Engineering, University of Texas at Austin, USA

(Received October 12, 2015, Revised March 8, 2016, Accepted March 15, 2016)

Abstract. An offshore wind turbine supported by a spar buoy floating platform is the subject of this study on tower and rotor extreme loads. The platform, with a 120-meter draft and assumed to be sited in 320 meters of water, supports a 5 MW wind turbine. A baseline model for this turbine developed at the National Renewable Energy Laboratory (NREL) is employed in stochastic response simulations. The support platform, along with the mooring system consisting of three catenary lines, chosen for loads modeling, is based on the “Hywind” floating wind turbine concept. Our interest lies in gaining an understanding of the dynamic coupling between the support platform motion and the turbine loads. We first investigate short-term response statistics using stochastic simulation for a range of different environmental wind and wave conditions. From this study, we identify a few “controlling” environmental conditions for which long-term turbine load statistics and probability distributions are established.

Keywords: spar platform; offshore wind energy; loads; stochastic simulation

1. Introduction

In recent years, there have been significant developments in wind energy development and wind turbine technologies both onshore as well as offshore. Wind turbines have grown considerably in size; wind farms with numerous such turbines have thus far been located on land and in shallow waters, where the turbines are bottom-supported. The potential for even more offshore wind energy development is great in many parts of the world. However, at most offshore sites in the United States where the wind resources are good, water depths are also great even at relatively short distances from the coast. Offshore wind energy development at such sites cannot rely on conventional bottom-supported wind turbines. In deep waters, floating wind turbines may offer an attractive solution. The difficulties in selecting a floating wind turbine are that of having a stable support platform with acceptable motions, while also keeping costs down. Floating platforms such as spar buoys are, then, good candidates for consideration. Indeed, several studies are underway to investigate their feasibility with regard to performance, economics, and construction. By virtue of its slender and deep draft, a spar buoy can easily fulfill demands on static stability; wave loads, too, are moderate on these platforms.

The consideration of spar floating platforms for offshore wind turbines has been the subject of

*Corresponding author, Professor, E-mail: lmanuel@mail.utexas.edu

several studies in recent years. Jonkman (2007) discussed performance comparisons of spar-supported floating turbines with those of other platforms. Shin (2011) reported on 1:128 model tests for different sea states that were based on the the OC3-Hywind platform. Platform motions and response amplitude operators (RAOs) were estimated from the tests in order to the assess the dynamic performance of the system. Browning *et al.* (2011) reported on the use of the DeepCwind 1:50 scale test data to calibrate and validate a model used with the FAST tool to represent a spar buoy floating wind turbine. Chen and Yu (2013) discussed results from simulations of two different spar platforms modified from the OC3-Hywind system. Different pre-tension levels in the mooring system were used and response characteristics were studied against a semi-submersible platform and a tension leg platform system. The same 5-MW turbine was supported by each floating platform system; operational and extreme environmental conditions were studied. Various design load cases were studied; a key finding was that significant platform pitch motions occurred for above-rated wind speeds when conventional pitch control employed in land-based turbines was employed. In one of the most comprehensive studies to date on spar platforms for offshore wind turbines, Karimirad (2011) offered numerous insights related to dynamic characteristics of these systems and, especially, on the role of control, aerodynamic damping, hydrodynamic damping, etc. on the performance of catenary as well as taut mooring systems. Interesting discussions on instabilities of such systems were discussed. Various limit states, external environmental conditions, and design load cases were studied in detail. Results based on these various studies are also documented in related works (Karimirad and Moan 2011, Karimirad and Moan 2012).

One of the challenges in the design of any offshore wind turbine system is the ability to predict loads and the resulting dynamic response of the coupled wind turbine and platform system. In the offshore environment, additional load sources (to those experienced by land-based turbines) impart new and difficult challenges for wind turbine analysts. Our objective here is to evaluate extreme loads for a spar buoy-supported floating offshore wind turbine at a site for which environmental data on wind and waves are available. Accurate load prediction depends on proper modeling of the stochastic processes describing the inflow turbulence and the waves as well as on realistic models of the turbine and the support structure. We employ TurbSim (Jonkman and Buhl Jr. 2007) for the inflow turbulence simulation and carry out turbine dynamic response simulations using FAST (Jonkman and Buhl Jr. 2005); FAST allows stochastic description of the aerodynamic as well as the hydrodynamic loads. Our study is focused on computing loads on a utility-scale 5 MW wind turbine model with a hub height of 90 meters that is supported on a spar buoy platform. The entire structure is assumed to be at located at a site with a water depth of 320 meters. To identify critical wind-wave conditions that can control long-term extreme loads, we study time histories, power spectra, response statistics, and probability distributions of loads. Extremes of platform motions as well as of tower and blade loads are studied. While the present study only addresses “short-term” extreme load probability distributions (conditional on selected wind speed and wave height combinations), findings from this study can be useful in addressing design load cases where such short-term load distributions are integrated with the likelihood of different environmental conditions to yield long-term loads associated with return periods on the order of 50 years.

2. Turbine and platform model for simulation

2.1 Turbine model and simulation procedure

The wind turbine considered in this study is the NREL 5MW offshore baseline wind turbine model (Jonkman *et al.* 2009), which is a representative utility-scale multi-megawatt turbine that has also been adopted as the reference model for the integrated European Upwind research program. This model does not correspond to any single commercially manufactured turbine, but it is a realistic representation of a three-bladed upwind 5 MW wind turbine; its properties are drawn from and extrapolated based on operating machines and conceptual studies. A rating of 5 MW was chosen because it is assumed to be the minimum rating at which deepwater offshore wind turbines can be cost-effective. The rotor diameter for this 5 MW machine is 126 m; the hub height is 90 m and the maximum rotor speed is 12.2 rpm. The hub-height rated wind speed for the turbine is 11.2 m/s. The tower is modeled as a cantilever; its fixed base is coincident with the top of the supporting spar buoy platform. The tower base is at an elevation of 10 m above the SWL (still water level) where the tower's diameter is 6.5 m, which also matches the diameter of the top of the spar buoy platform. The cylindrical tower's base thickness is 0.027 m; the tower tapers linearly towards the top where its diameter reduces to 3.87 m and its thickness to 0.019 m. The resulting integrated tower mass is 249,718 kg with a center of mass located 43.4 m above SWL. A damping ratio 1% of critical is specified for all the vibrational modes of the tower. See Fig. 1 for a schematic diagram of the wind turbine and the supporting spar buoy platform. For the stochastic inflow velocity field simulations, Kaimal power spectra are employed for the three spatial components and an exponential coherence function is employed for the longitudinal wind velocity component; the simulations are carried out using the computer program, TurbSim (Jonkman and Buhl, Jr. 2007).

2.2 Spar buoy platform model

The floating platform model considered is a spar buoy that achieves stability by using ballast to lower the center of gravity (CG) below the center of buoyancy (CB). See Fig. 1. Whenever an overturning moment is produced due to wind or wave forces, a counteracting moment is generated between the center of gravity and the center of buoyancy which acts to return the spar buoy to its original position (Sclavounos *et al.* 2007). The draft of the platform is 120 m; the top and bottom portions of the spar buoy are made up of two cylinders of different diameters that are joined via a linearly tapered conical section. The top cylindrical section has a diameter of 6.5 m and extends down to 4 m below the SWL; the linearly tapered conical section extends from there to 12 m below the SWL, where the diameter increases to 9.4 m. The lower cylindrical portion of the spar buoy platform maintains this same diameter of 9.4 m. The resulting spar buoy platform has a centre of mass located at a depth 89.9 m below the SWL. The mass of the floating platform including ballast is 7,466,330 kg. The moment of inertia associated with both roll and pitch of the platform about its center of mass is 4,229,230,000 kg-m² and the moment of inertia associated with yaw of the platform about its center of gravity is 164,230,000 kg-m². The water depth at the selected site is taken to be 320 m. The spar buoy is modeled as a rigid body with six degrees of freedom; it is connected to the sea floor by multi-component catenary mooring lines. These mooring lines are attached to the spar buoy at the fairleads.

The spar buoy platform is moored with a system of three catenary lines in order to prevent it from drifting. The three lines are modeled as homogeneous with properties derived as weighted average values of the line's mass, weight and stiffness. The mooring system damping, including the hydrodynamic drag and line-to-seabed drag, is neglected. Each of the three lines has an unstretched length of 902.2 m, a diameter of 0.09 m. The lines are at an angle of 120 degrees with

respect to each other. The three mooring lines are anchored 320 m below the still water level. One of the lines is assumed to be directed along the positive X-axis (in the XZ plane). The lines are attached to the hull near its center of pitch for low dynamic loading such that when the platform deflects, the movement takes place in a plane of symmetry of the mooring system, the resultant horizontal force also occurs in this plane, and the behavior of the mooring system is two-dimensional. The mooring system is augmented with a yaw spring to achieve the proper overall yaw stiffness; this additional yaw spring has a stiffness of 98,340,000 N-m/rad. The fairleads are located 5.2 m from the platform center line. The mooring line anchors are located at a radius of 853.87 m from the platform center line. The mooring lines used have an equivalent apparent weight in fluid per unit length of 698.094 N/m, and an equivalent extensional stiffness of 384,243,000 N.

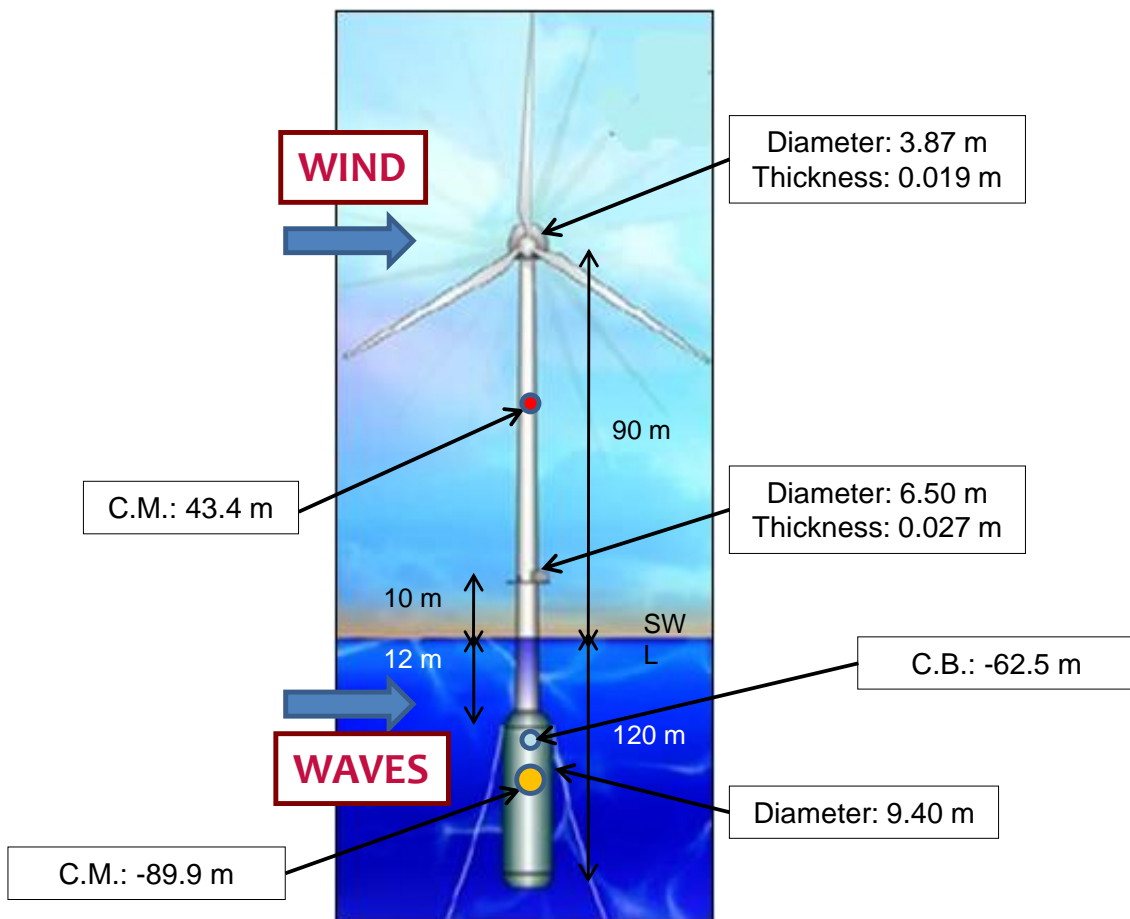


Figure not to scale

Fig. 1 Schematic diagram of the spar buoy-supported floating offshore wind turbine (modified based on Jonkman 2007)

3. Loading and environmental conditions

3.1 Hydrodynamic forces on the floating platform

Hydrodynamic loads for the floater result from the dynamic pressure of the water over the wetted surface of the support platform. Due to hydrodynamic loading on the support platform, impedance forces including the effects of added mass and damping become important. The added mass component of the hydrodynamic forces is relevant since the density of water is comparable with the density of the structural materials; this is in contrast to the aerodynamic loading on the wind turbine where the effects of added mass can be neglected since the density of air is much lower than that of the materials that make up the primary structure.

For the hydrodynamic loading on the support structure, irregular long-crested (uni-directional) waves are simulated using a JONSWAP spectrum (Det Norske Veritas 2007). Forces resulting from fluid-structure interaction include frequency-dependent added-mass and damping matrices arising from linear wave radiation using WAMIT. FAST employs these frequency-dependent effects to derive hydrodynamic loads. The FAST simulator employed accounts for the hydrodynamic loads by first simulating a random sea surface elevation process, and then computing appropriate wave kinematics and inertia and drag force components (Jonkman and Buhl, Jr. 2005).

3.2 Reference site and environmental conditions

As per IEC 61400-3 (International Electrotechnical Commission, 2009) consideration of some design load cases needs to be based on site-specific external conditions. This study is carried out for a site (Stevenson Weather Station) assumed to be located at 61°20' N latitude, 0°0' E longitude near the Shetland Islands, northeast of Scotland. This location is considered because of its fairly extreme wind and wave conditions that may be expected to experience intense wind- and wave-induced loading on any deepwater floating wind turbine. We assume that the environment is described by the ten-minute average mean wind speed, V at the hub height, the significant wave height, H_s (four times the standard deviation of the sea surface elevation process), and the wave peak spectral period, T_p . The joint probability distribution for V , H_s , and T_p may be represented as shown in Fig. 2 where V - H_s and H_s - T_p bivariate distributions are presented, based on 13 years of data (comprising 37,992 samples for 3-hour reference periods). The samples for the three environment variables were grouped in bins; the bin size for mean wind speed, V , significant wave height, H_s , and spectral period, T_p , are 1.399 m/s, 1 m, and 1.408 s, respectively, as described by Jonkman (2007). Even though the water depth at the Stevenson site was lower than 320 meters (the water depth used in the loads studies for the floating offshore wind turbine considered here), the joint environmental distribution at this site is employed since it is thought to be representative of deepwater sites that would be candidates for any floating offshore wind turbine.

The selection of triads of V , H_s and T_p values for turbine loads analysis is done by first choosing six values of mean wind speed, V , over the entire operating range of the wind turbine from cut-in to cut-out winds ($V_{in} = 3 \text{ m/s} < V < V_{out} = 25 \text{ m/s}$). Then, for each wind speed, three different significant wave height values are chosen, corresponding to low, medium, and high values of H_s for the given V value, based on the joint V - H_s distribution. The selected wave peak spectral period, T_p , is that based on the conditional distribution of T_p on H_s and V ; the conditional expected value

of T_p given H_s and V is used for each of the selected sets of environmental conditions used in subsequent analyses. A total of eighteen sea states are selected for the turbine stochastic response simulations; Table 1 summarizes the V , H_s and T_p values for these selected sea states.

4. Stochastic response simulations

Fifteen ten-minute simulations of the turbine response were carried out for each of the selected eighteen sea states identified in Table 1; each ten-minute response series resulted from separate wind velocity field simulation using TurbSim, followed by turbine response simulation using FAST. Time series data in the ten-minute time series were obtained with 20 Hz sampling; statistics including the minimum, maximum, mean, and standard deviation for each response process were studied. The load variables studied include the tower base fore-aft bending moment (TwrBsMyt), the tower base side-to-side bending moment (TwrBsMxt), the blade root out-of-plane bending moment (RootMyc1), and the blade root in-plane bending moment (RootMxc1). The tower top deflection in the fore-aft direction (TTDspFA) and the blade tip out-of-plane deflection (OoPDefl1) are also studied. The platform motions studied include surge, sway, heave, roll, pitch, and yaw.

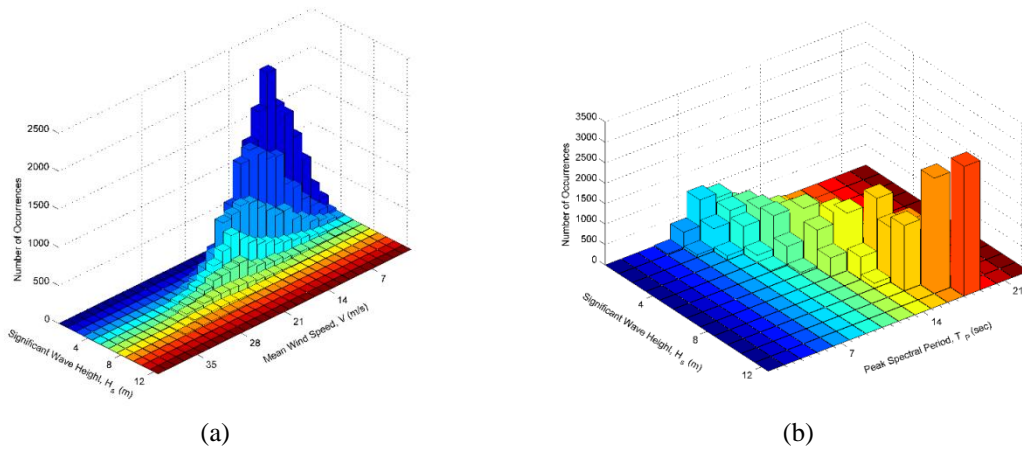


Fig. 2 Joint distributions (based on data from the Stevenson Weather Station) showing (a) hub-height ten-minute mean wind speed versus significant wave height; and (b) significant wave height versus peak spectral period

Table 1 Sea states selected for the turbine response stochastic simulations

V (m/s)	Low wave height		Medium wave height		High wave height	
	H_s (m)	T_p (s)	H_s (m)	T_p (s)	H_s (m)	T_p (s)
6.30	0.5	8.77	3.5	14.40	6.5	17.60
9.10	0.5	7.78	4.5	15.31	7.5	16.19
11.89	0.5	7.08	3.5	13.39	6.5	17.60
14.69	1.5	8.42	5.5	15.86	8.5	16.19
17.49	1.5	8.23	5.5	14.98	8.5	18.31
21.69	1.5	7.74	5.5	13.96	9.5	19.01

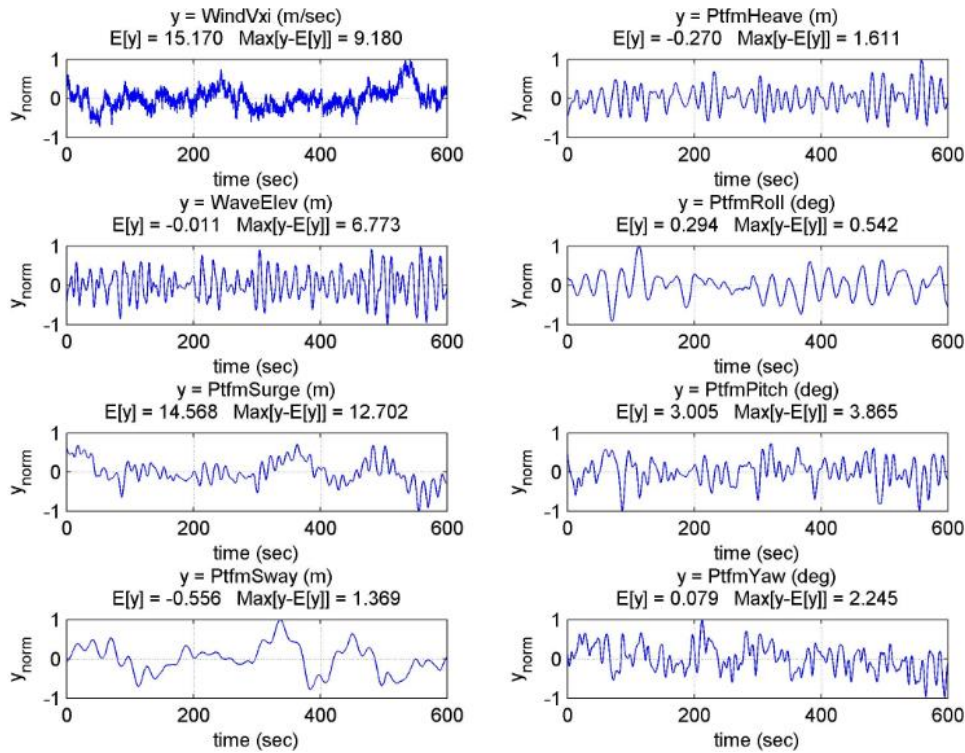


Fig. 3 Time series of the hub-height longitudinal wind speed, the sea surface elevation, and the platform motions for the floating offshore wind turbine for $V = 14.69$ m/s, $H_s = 8.5$ m, $T_p = 16.19$ s

Following the preliminary study of the eighteen sea states, two combinations of mean hub height wind speed, V , significant wave height, H_s , and mean spectral wave period, T_p that yielded large loads are identified and studied in depth with a view to assessing extreme load distributions for those sea states based on a large number of simulations. Accordingly, 1200 simulations were carried out for two (V, H_s, T_p) triads— $V = 14.69$ m/s, $H_s = 8.50$ m, $T_p = 16.19$ s and $V = 17.49$ m/s, $H_s = 8.50$ m and $T_p = 18.31$ s—and the extreme load distributions for these sea states are discussed separately. The motivation for studying such “short-term” load distributions is that they directly influence characteristic loads associated with long return periods (on the order of 50 years) needed in addressing an ultimate limit state for design.

5. Numerical studies

5.1 Time series

Fig. 3 shows time series, normalized such that for any response, $y(t)$, of interest, what is plotted is $[(y(t)-E[y])/max\{|y|\}]$ versus time, t . Time series presented are for the hub-height longitudinal wind speed, the sea surface (wave) elevation, and the six platform motions, surge, sway, heave,

roll, pitch and yaw, that describe the rigid body motion of the platform. These various time series correspond to the sea state where $V = 14.69$ m/s, $H_s = 8.5$ m, and $T_p = 16.19$ sec. From the time series, it may be noted that there is a dominant long period evident in the platform surge and sway motions. The heave, roll, pitch, and yaw degrees of freedom exhibit significantly greater high-frequency content. The maximum platform surge motion is 27.3 m; sway motion is relatively small in comparison mainly because the direction of the wave excitation forces and the coincident wind direction are aligned with the platform surge degree of freedom. There is some coupling or dynamic interaction between the surge and pitch modes; hence, the time series show considerable pitching of the system along with the large surge motions.

Time series for various turbine response quantities are presented in Fig. 4 along with the hub-height longitudinal wind speed and the sea surface elevation. It is clear that the tower base fore-aft bending moment (TwrBsMyt) exhibits similar dynamics to that of the tower top fore-aft displacement (TTDspFA). Also, the blade root out-of-plane bending moment for Blade 1 (RootMyc1) shows similar dynamic characteristics to that of the out-of-plane tip deflection of the same blade (OoPDefl1). Time series of the blade-root in-plane bending moment (RootMxc1) and the tower base side-to-side bending moment (TwsBsMxt) exhibit comparatively greater high-frequency content.

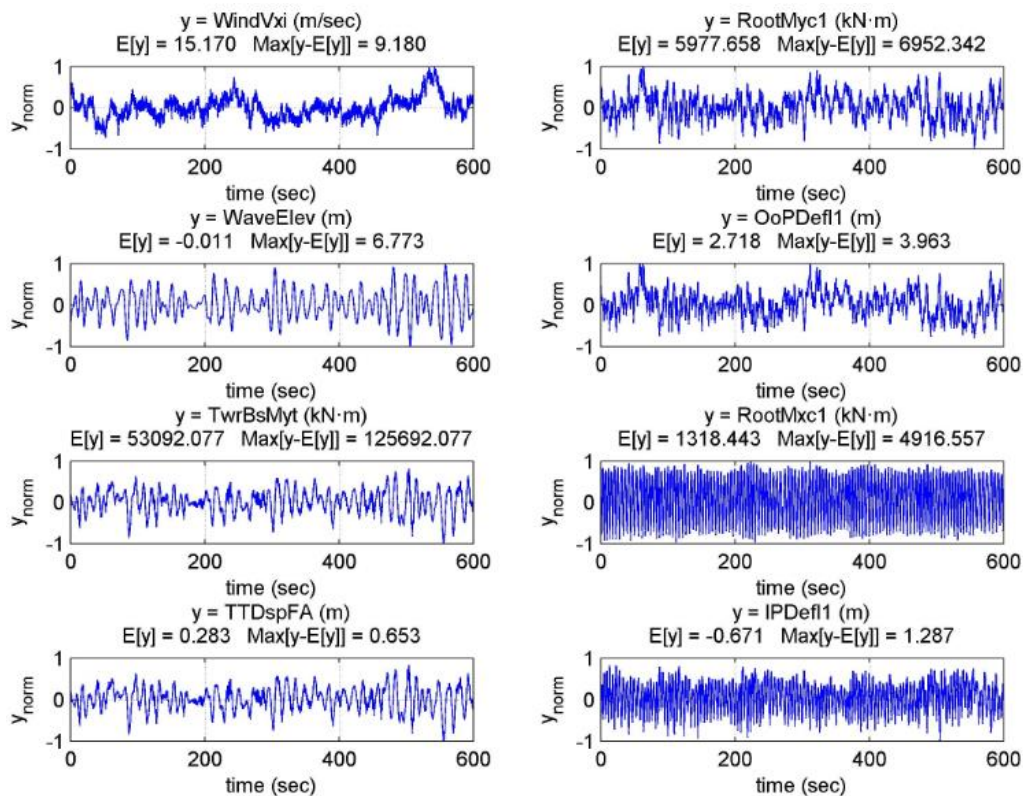


Fig. 4 Time series of the hub-height longitudinal wind speed, the sea surface elevation, and various turbine tower and blade response quantities for the floating offshore wind turbine for $V = 14.69$ m/s, $H_s = 8.5$ m, $T_p = 16.19$ s

5.2 Summary statistics

To compare the relative importance of different wind speeds on load extremes, it is of interest to study load extreme statistics as a function of wind speed. From limited simulations, we can identify which wind speeds cause greater turbine loads on average and, equally important, which ones lead to greatest load variability. Even if loads realized for some wind speeds are not among the largest on average, if the variability in load extremes from simulations with those wind speeds is large, such winds can have a significant influence on load distribution tails and, hence, on extrapolated very large loads associated with low probabilities of exceedance.

Table 2 summarizes ensemble statistics from fifteen ten-minute simulations of the tower base fore-aft bending moment (TwrBsMyt) for all the eighteen selected sea states. The largest ten-minute load extremes are seen to result near the mean wind speed bin of 14.69 m/s, and with the associated significant wave height of 8.5 m and wave spectral peak period of 16.19 sec. The mean values of the tower base fore-aft bending moment do not vary greatly for a given mean wind speed even with large changes in the significant wave height. This suggests that for this spar buoy-supported offshore floating wind turbine, the waves do not contribute much towards influencing extreme loads; it is mostly the winds that do so. The mean tower fore-aft bending moment increases as the mean wind speed increases from 6.30 m/s to 11.89 m/s; thereafter, it decreases monotonically with wind speed. This is as expected for this pitch-regulated wind turbine with a rated wind speed of 11.2 m/s. For the tower base fore-aft bending moment, the controlling wind speeds lie in the range from 11.89 m/s to 17.49 m/s with perhaps the dominant winds being closest to mean wind speed of 14.69 m/s. The standard deviation of TwrBsMyt and the extreme values show monotonically increasing trends with increase in wave height at all wind speeds.

Table 2 Ensemble statistics of the tower base fore-aft bending moment from fifteen ten-minute simulations for the selected eighteen sea states

V (m/s)	H_s (m)	T_p (sec)	Tower base fore-aft bending moment (TwrBsMyt) Statistics			
			Max (MN-m)	Min (MN-m)	Mean (MN-m)	Std. Dev. (MN-m)
6.30	0.5	8.77	65.57	7.00	30.50	9.43
	3.5	14.40	79.94	-16.23	30.37	15.17
	6.5	17.60	106.31	-42.68	31.23	24.12
9.10	0.5	7.78	105.32	13.36	60.57	17.02
	4.5	15.31	127.01	-10.54	59.37	21.75
	7.5	16.19	150.39	-39.10	59.56	30.10
11.89	0.5	7.08	118.43	17.88	72.09	17.00
	3.5	13.39	134.39	4.77	71.64	21.38
	6.5	17.60	154.47	-14.45	70.29	27.58
14.69	1.5	8.42	118.04	1.15	56.02	18.49
	5.5	15.86	143.58	-19.48	55.91	26.00
	8.5	16.19	161.10	-44.16	55.98	34.01
17.49	1.5	8.23	105.22	-2.83	46.14	15.88
	5.5	14.98	120.01	-27.68	45.63	24.36
	8.5	18.31	155.27	-56.40	45.43	32.16
21.69	1.5	7.74	89.95	-9.21	38.83	14.54
	5.5	13.96	121.43	-39.04	38.47	25.01
	9.5	19.01	151.49	-67.25	38.41	34.43

Other tower-related response variables such as *TwrBsMxt* and *TTDspFA* show similar overall trends to that of *TwrBsMyt*. Blade-related response variables such as *OoPDef11*, *RootMyc1*, and *RootMxc1* have highest extreme values for wind speeds between 11.89 m/s and 14.69 m/s. They do not vary much with wave height. The observations made above, especially the remark related to the influence of aerodynamic loading on the turbine system loads, need to be considered with the understanding that the turbine is in an operating state for all the wind speeds considered; in a parked state, the absence of aerodynamic damping will influence its effects. We also note that collective pitch control is assumed for the turbine in this study; changes in the control system will affect the relative influence of aerodynamic versus hydrodynamic loading on the system response.

Summary statistics for the platform surge motion are presented in Table 3. For a given mean wind speed, the platform mean surge motion does not change very much with change in significant wave height, the surge motion of the spar buoy platform is mainly governed by the wind. Unlike the fore-aft tower base bending moment, all the summary statistics (including mean, standard deviation, and extremes) of platform surge platform surge do not vary much for different significant wave height and show no monotonic trends. Surge motions are highest close to the rated wind speed of 11.2 m/s.

The wind speeds where the largest turbine loads occur are of obvious interest; these conditions tend to be associated with the rare loads that are of importance in design. Empirical short-term load distributions need to be accurately estimated in these important wind speed bins. From Tables 2 and 3, it is clear that mean wind speeds bins below 11.89 m/s do not cause large turbine loads; they also do not exhibit large variability.

Table 3 Ensemble statistics of the platform surge from fifteen ten-minute simulations for the selected eighteen sea states

<i>V</i> (m/s)	<i>H_s</i> (m)	<i>T_p</i> (sec)	Platform Surge Statistics			
			Max (m)	Min (m)	Mean (m)	Std. Dev. (m)
6.30	0.5	8.77	14.21	3.40	8.61	2.65
	3.5	14.40	15.88	1.92	8.59	2.96
	6.5	17.60	17.22	0.83	8.80	3.34
9.10	0.5	7.78	26.85	7.52	17.04	4.88
	4.5	15.31	28.55	6.77	16.69	4.76
	7.5	16.19	28.51	5.19	16.81	5.05
11.89	0.5	7.08	29.67	11.06	20.11	4.45
	3.5	13.39	30.42	10.34	20.07	4.33
	6.5	17.60	29.47	9.75	19.55	4.13
14.69	1.5	8.42	24.43	7.64	15.46	3.85
	5.5	15.86	26.13	5.95	15.44	4.17
	8.5	16.19	26.55	5.20	15.44	4.27
17.49	1.5	8.23	19.25	6.61	12.45	2.68
	5.5	14.98	19.65	5.73	12.32	2.73
	8.5	18.31	22.03	3.57	12.27	3.32
21.69	1.5	7.74	16.29	5.17	10.20	2.07
	5.5	13.96	17.19	3.77	10.03	2.33
	9.5	19.01	18.84	1.78	9.99	3.12

These low mean wind speed bins are not generally important in statistical loads extrapolation for design and a minimal effort in terms of simulation may be justified for these mean wind speed bins. On the other hand, wind speeds at and above the rated wind speeds are likely most important in long-term load prediction. We will return to accurate load distribution estimation based on a very large number of simulations for two load types and for two different sea states where the wind speed is in this important range.

5.3 Short-term load distributions

Short-term distributions for various turbine response variables based on fifteen ten-minute simulations for a mean wind speed of 14.69 m/s, a significant wave height of 8.5 m, and a wave peak spectral period of 16.19 sec are considered next. Cumulative distribution plots for the simulated hub-height longitudinal wind speed, the sea surface elevation, and various turbine response variables are presented in Fig. 5. Platform surge motion is seen to experience the greatest variability for the selected environmental state. We can see low variability in the turbine in-plane loads. The turbine blade and tower response variables exhibit lower variability compared to the platform motions. The tails of these various short-term distributions do indicate greater variability in the tails for the tower- and blade-related response variables. This suggests that turbine tower and blade load extremes and long-term load prediction may not be established using only fifteen simulations. A greater number of simulations is needed for estimating such short-term load distributions for each important sea state. This issue is addressed later.

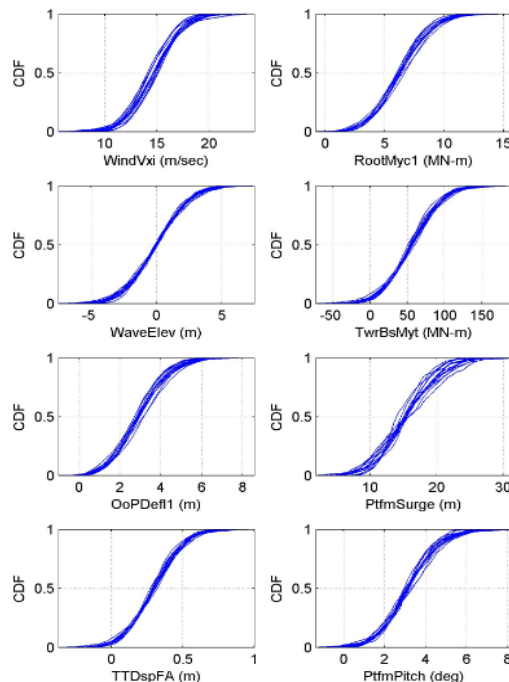


Fig. 5 Cumulative distribution functions of the hub-height longitudinal wind speed, the sea surface elevation, and various turbine response variables based on fifteen ten-minute simulated time series with input environmental variables, $V = 14.69$ m/s, $H_s = 8.5$ m, and $T_p = 16.19$ s

5.4 Power spectra

Power spectral density function plots for the simulated hub-height longitudinal wind speed, the sea surface elevation, and various turbine response variables are presented in Fig. 6 for a single ten-minute simulation with input environmental variables, $V = 14.69$ m/s, $H_s = 8.5$ m, and $T_p = 16.19$ s. It is evident that the background (low-frequency) component from the wind contributes differently to the various turbine response measures studied compared to relevant resonant components. For the environmental conditions considered here, the wave energy is largest around 0.06 Hz—i.e., at frequencies higher than those of the slow platform motions associated, say, with surge (around 0.008 Hz). The effectiveness of the coupled dynamic system is evident from the energy concentrated at low natural system frequencies in contrast to the environmental wave conditions. For frequencies of excitation well above any system natural frequency, the mass cannot “follow” the excitation; consequently, the response level is low and the response is almost in counter-phase with the excitation and the inertia of the system dominates the response. Greater low-frequency content is observed for the turbine platform motions, PtfmSurge and PtfmPitch, as well as for TTDspFA, and OoPDefl1 compared to that for the tower and blade bending moments, TwrBsMyt and RootMyt1, respectively.

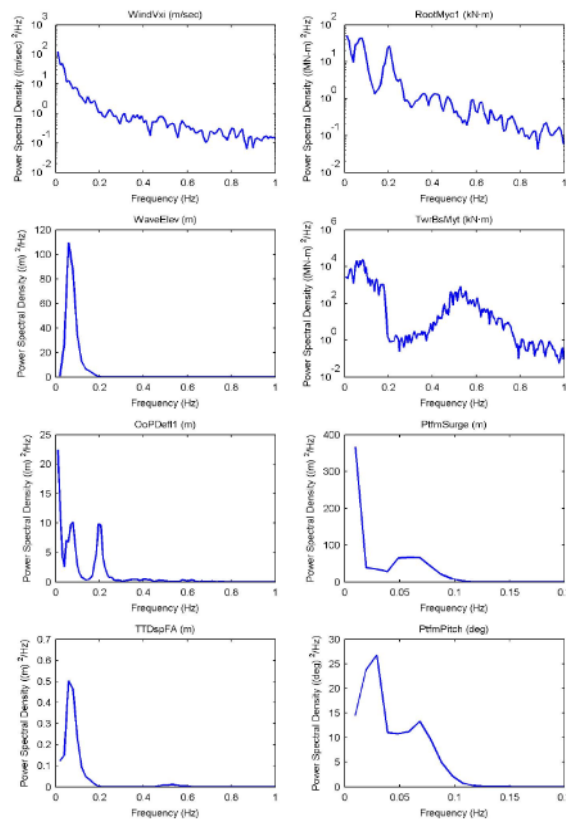


Fig. 6 Power spectral density functions of the hub-height longitudinal wind speed, the sea surface elevation, and various turbine response variables for a single ten-minute simulated time series with input environmental variables, $V = 14.69$ m/s, $H_s = 8.5$ m, and $T_p = 16.19$ s

The influence of waves on turbine response is studied by considering significant wave heights of 0.5 m, 3.5 m and 6.5 m, while the mean wind speed is held constant at 11.89 m/s. In Fig. 7, power spectral density function plots for the simulated hub-height longitudinal wind speed, the sea surface elevation, and various turbine response variables are presented. Blade loads show relatively little sensitivity to change in wave height. Power spectra for tower loads, too, show no significant influence of change in wave height, except at frequencies below 0.2 Hz where the wave energy is dominant; sea surface elevation peak spectral frequencies are 0.14 Hz, 0.074 Hz, and 0.056 Hz, respectively, for significant wave heights of 0.5, 3.5 and 6.5 m.

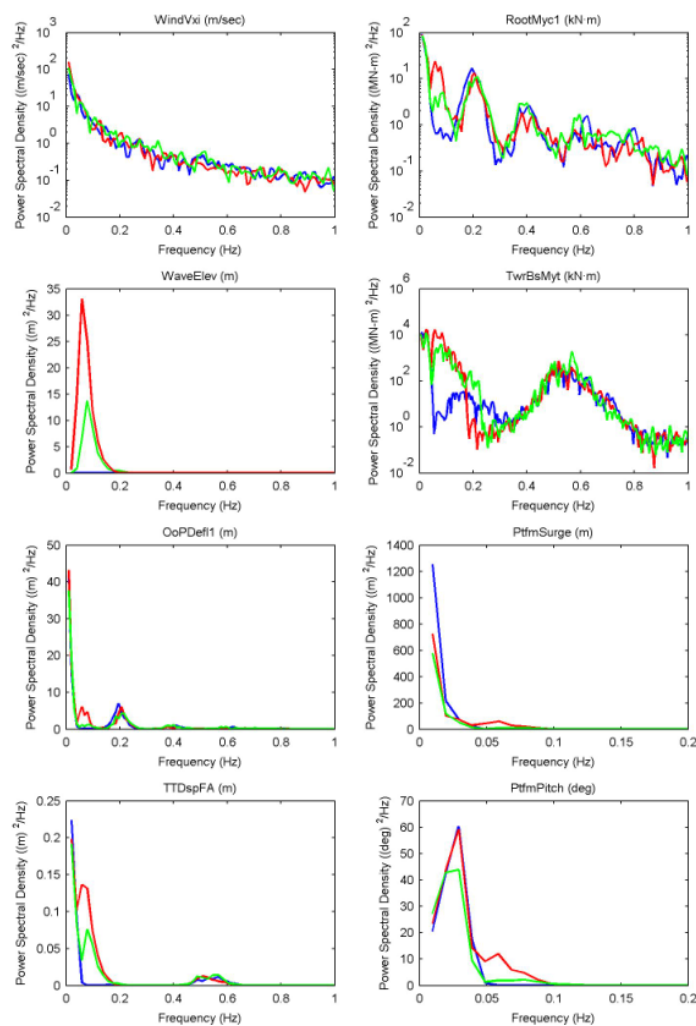


Fig. 7 Variation in power spectral density functions of the hub-height longitudinal wind speed, the sea surface elevation, and various turbine response variables as the significant wave height is changed for a fixed ten-minute average longitudinal hub-height mean wind speed of 11.89 m/s (blue: $H_s = 0.5$ m; green: $H_s = 3.5$ m; red: $H_s = 6.5$ m)

The influence of change in wind conditions on turbine response is studied by considering hub-height ten-minute average longitudinal wind speeds of 6.30 m/s, 11.89 m/s, and 21.69 m/s, while the significant wave height is held constant at 6.5 m. In Fig. 8, power spectral density function plots for the simulated hub-height longitudinal wind speed, the sea surface elevation, and various turbine response variables are presented. It can be seen that, in general, blade and tower loads have increased energy (variance) with increase in wind speed. Even though maximum tower bending moments are higher for wind speeds around rated (Table 2), the variance (equal to the area under the power spectral density function plot versus frequency) is smaller at those wind speeds than at 21.69 m/s (Fig. 8). Important peaks in the power spectra for the blade loads are seen at 1P (corresponding to the rotor rotation rate which is 0.2 Hz at and above the rated wind speed) and multiples (such as 3P = 0.6 Hz). Peaks in the power spectra plots for the turbine response shift more noticeably with variation in wind speed than they do with variation in wave height (Fig. 7).

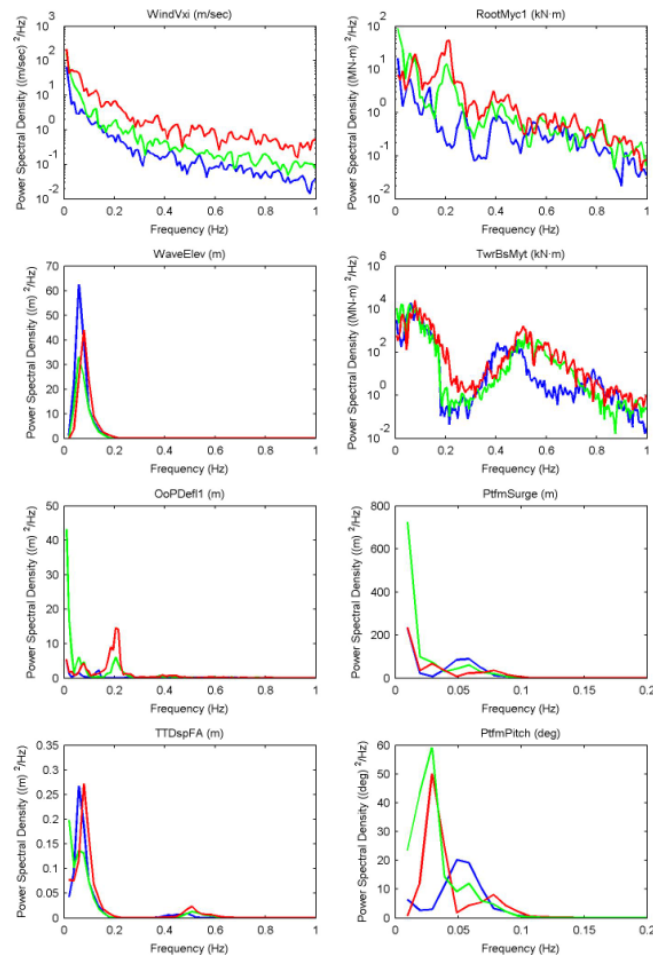


Fig. 8 Variation in power spectral density functions of the hub-height longitudinal wind speed, the sea surface elevation, and various turbine response variables as the ten-minute average hub-height longitudinal wind speed is changed for a fixed significant wave height of 6.5 m (blue: $V = 6.30$ m/s; green: $V = 11.89$ m/s; red: $V = 21.69$ m/s)

5.5 Turbine load probability distributions

It is of interest to study “short-term” probability distributions for loads on the offshore wind turbine for specific critical combinations of wind speed and wave height. Based on simulations results presented, critical combinations were selected as $V = 14.69$ m/s, $H_s = 8.50$ m (with $T_p = 16.19$ s) for the fore-aft tower bending moment at the tower bottom and $V = 11.89$ m/s, $H_s = 6.50$ m (with $T_p = 17.60$ s) for the blade root out-of-plane bending moment. For these sea states, a total of 1,200 ten-minute simulations were run. Fig. 9 shows estimates of the probability distributions for these two loads based on the simulations. It is often the case that, if the critical environmental conditions are identified correctly, rare load exceedance probabilities from such empirical probability distributions based on simulation may be directly related to characteristic loads needed in design for long return periods (Agarwal and Manuel 2008, Agarwal and Manuel 2009).

Even though the probability distribution curves for tower and blade loads in Fig. 9 were presented for a single sea state identified as critical in each case, it is of interest to also evaluate other potentially interesting sea states (or V and H_s combinations) close to these selected combinations and compare load variability and maxima for any such alternative environmental conditions. Table 4 summarizes tower base fore-aft and blade root out-of-plane bending moment statistics based on 1,200 ten-minute simulations for such alternative wind-wave environmental conditions instead of those presented in Fig. 9. Gross second order-statistics (such as the load standard deviations) are higher for the $V = 14.69$ m/s and $H_s = 8.50$ m sea state by 7.1% and 12.6% for tower and blade loads, respectively, compared to the other sea state considered for each load. The tower load maxima are higher by more than 10% for the $V = 14.69$ m/s and $H_s = 8.50$ m case compared to the alternative $V = 17.49$ m/s, $H_s = 8.50$ m case; whereas the blade load maxima are higher by only about 2% for the $V = 11.89$ m/s and $H_s = 6.50$ m case versus the $V = 14.69$ m/s and $H_s = 8.50$ m case.

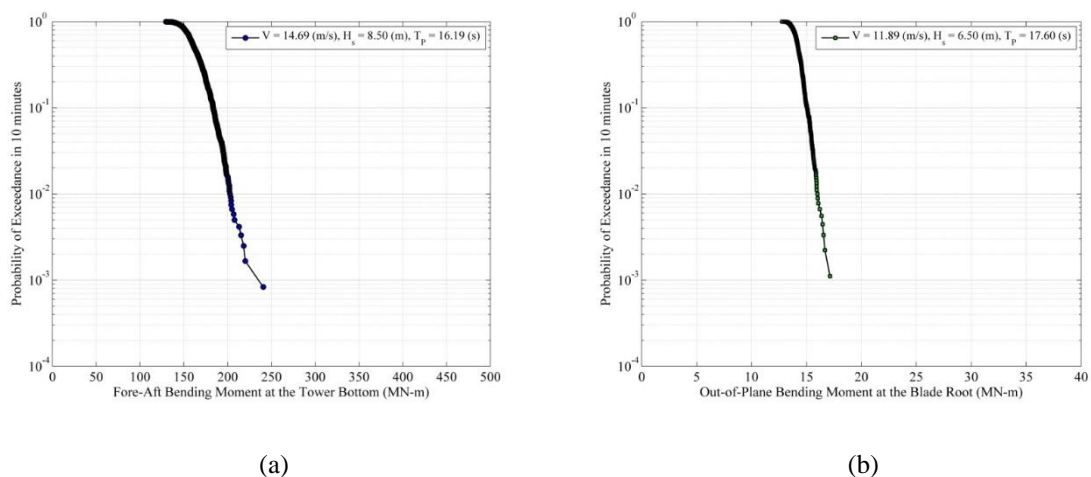


Fig. 9 Probability of exceedance plots (based on 1,200 ten-minute simulations) for (a) the tower base fore-aft bending moment for $V = 14.69$ m/s, $H_s = 8.5$ m, $T_p = 16.19$ s; and (b) the blade root out-of-plane bending moment for $V = 11.89$ m/s, $H_s = 6.5$ m, $T_p = 17.30$ s

Table 4 Ensemble statistics of the tower base fore-aft bending moment and the blade root out-of-plane bending moment based on 1,200 ten-minute simulations for two selected sea states in each case

$$PF(max) = (Max - Mean)/Std. Dev.$$

Load	V (m/s)	H_s (m)	T_P (s)	Max (MN-m)	Min (MN-m)	$Mean$ (MN-m)	$Std. Dev.$ (MN-m)	Skewness	Kurtosis	PF (max)
TwrBsMyt	14.69	8.50	16.19	163.96	-49.14	55.58	34.44	0.03	2.95	3.15
	17.49	8.50	18.31	146.59	-51.71	45.83	31.99	0.03	2.95	3.15
RootMyc1	11.89	6.50	17.30	14.30	1.98	8.27	1.94	-0.11	2.84	3.11
	14.69	8.50	16.19	14.00	-0.07	6.27	2.22	0.21	2.90	3.48

This suggests that the extreme tower loads are clearly higher for mean wind speeds around 14.69 m/s; however, extreme blade loads are large for a wider range of wind speeds and may require more careful identification of critical environmental conditions and associated turbine response simulations. It is interesting to note that even though there are significant differences in load variability (i.e., load standard deviation) in the two sea states studied for the blade loads with the $V = 14.69$ m/s and $H_s = 8.50$ m case loads exceeding the $V = 11.89$ m/s and $H_s = 6.50$ m case loads by a large margin, it is the $V = 11.89$ m/s and $H_s = 6.50$ m case that yields the larger extremes; this is due mainly to the higher mean load closer to the rated wind speed that falls by more than 20% when the wind speed changes from 11.89 m/s to 14.69 m/s. For tower loads, both the mean and the standard deviation are larger for the $V = 14.69$ m/s and $H_s = 8.50$ m case versus the $V = 17.49$ m/s and $H_s = 8.50$ m case; hence, the maxima are governed by the $V = 14.69$ m/s and $H_s = 8.50$ m case.

6. Conclusions

The coupled hydrodynamic and aero-elastic response of the selected spar buoy-supported offshore wind turbine was studied in time-domain stochastic simulations. Motions as well as tower and blade loads extremes were studied. It was found that the response and loads experienced by this offshore floating wind turbine were influenced to a greater degree by the input wind conditions than by the waves. Due to the mean wind speed on the rotor, there are significant mean surge motions of the spar buoy platform supporting the floating offshore wind turbine. Platform motions exhibited greater variability compared to the tower and blade loads. Fifteen ten-minute response simulations for several different sea states were analyzed to help identify critical environmental conditions that could potentially cause large loads. By carrying out a much larger number of simulations (1,200) for a few sea states, extreme tower loads were found to be higher for ten-minute hub-height longitudinal wind speeds of 14.69 m/s with the accompanying highest possible wave height for that wind speed; extreme blade loads were found to be higher for a hub-height wind speed of 11.89 m/s, closer to the rated wind speed for the turbine. Long-term load distributions and derivation of characteristic loads associated with return periods on the order of 50 years need to be focused near these noted mean wind speeds.

Acknowledgments

The authors gratefully acknowledge the financial support provided by the National Science Foundation (by way of CAREER Award No. CMMI-0727989) and by Sandia National Laboratories (by way of Contract No. 743358). The authors also wish to acknowledge Dr. Jason Jonkman at the National Renewable Energy Laboratory for his assistance with the simulation program, FAST, and with the environmental data used in this study.

References

- Agarwal, P. and Manuel, L. (2008), "The Influence of the Joint Wind-Wave Environment on Offshore Wind Turbine Support Structure Loads", *J. Solar Energy Engineering including Wind Energy and Building Energy Conservation*, Transactions of the ASME, **130**(1), 031010, 11.
- Agarwal, P., and Manuel, L. (2009), "Simulation of offshore wind turbine response for ultimate limit states", *Eng. Struct.*, **31**(10), 2236-2246.
- Browning, J.R., Jonkman, J., Robertson, A. and Goupee, A.J. (2011), *Calibration and Validation of a Spar-Type Floating Offshore Wind Turbine Model using the FAST Dynamic Simulation Tool*, The Science of Making Torque from Wind, Journal of Physics: Conference Series 555, IOP Publishing.
- Chen, X. and Yu, Q. (2013), "Design requirements for floating offshore wind turbines", *Proceedings of the 32nd International Conference on Ocean, Offshore and Arctic Engineering*, OMAE2013-11365, Nantes, France.
- Det Norske Veritas. (2007), *Design of Offshore Wind Turbine Structures*, Offshore Standard DNV-OS-J101.
- International Electrotechnical Commission. (2009), *Wind Turbines – Part 3: Design Requirements for Offshore Wind Turbines*, IEC 61400-3, Ed. 1.
- Jonkman, B.J., and Buhl Jr., M.L. (2007), *TurbSim User's Guide*. Tech. Rep. NREL/TP-500-41136, National Renewable Energy Laboratory, Golden, CO.
- Jonkman, J.M. (2007), *Dynamics Modeling and Loads Analysis of an Offshore Floating Wind Turbine*. Ph.D. Dissertation, University of Colorado at Boulder.
- Jonkman, J.M., and Buhl Jr., M.L. (2005), *FAST User's Guide*. Tech. Rep. NREL/EL-500-38230, National Renewable Energy Laboratory, Golden, CO.
- Jonkman, J.M., Butterfield, S., Musial, W. and Scott, G. (2009), *Definition of a 5-MW Reference Wind Turbine for Offshore System Development*. Tech. Rep. NREL/TP-500-38060, National Renewable Energy Laboratory, Golden, CO.
- Karimirad, M. (2011), *Stochastic Dynamic Response Analysis of Spar-Type Wind Turbines with Catenary or Taut Mooring Systems*, Doctoral Thesis, Norwegian University of Science and Technology.
- Karimirad, M. and Moan, T. (2011), "Extreme dynamic structural response analysis of catenary moored spar wind turbine in harsh environmental conditions", *J. Offshore Mech. Arct. Eng. - ASME*, **133**(4), 041103.
- Karimirad, M. and Moan, T. (2012). "Wave- and wind-induced dynamic response of a spar-type offshore wind turbine", *J. Waterw. Port. Coastal. Ocean Eng.*, **138**(1).
- Sclavounos, P., Jonkman, J.M., Butterfield, S. and Musial, W. (2007), *Engineering Challenges for Floating Offshore Wind Turbines*, Tech. Rep. NREL/ CP-500-38776, National Renewable Energy Laboratory, Golden, CO.
- Shin, H. (2011), "Model Test of the OC3-Hywind Floating Offshore Wind Turbine", *Proceedings of the 21th International Offshore and Polar Engineering Conference*, Maui, Hawaii, USA.